Ocean Dynamics
DOI 10.1007/s10236-011-0455-y

Observations of estuarine circulation and solitary internal waves in a highly energetic tidal channel

Sjoerd Groeskamp · Janine J. Nauw · Leo R. M. Maas

Received: 4 February 2011 / Accepted: 9 June 2011

Abstract Despite vigorous tidal and wind mixing, observations in an estuarine tidal inlet in the Wadden Sea show that during part of the tidal cycle, vertical stratification and internal waves may still develop. Acoustic Doppler current profiler (ADCP) and conductivity, temperature, depth observations, collected over the past 6 years at 13 h anchor stations (ASs), reveal that these occur especially during slack tide, when there is little wind and large freshwater discharge from nearby Lake IJssel. Measurements with a moored ADCP show that in the same tidal phase, strong cross-channel circulation develops, which may suddenly reverse circulation sense due to passing density fronts. In the vertically stratified phase that follows after the front passage, propagating mode-one solitary internal waves are observed. These are resonantly generated during decelerating tidal ebb currents when the (shear) flow passes a transcritical regime (Froude number equal to 1). A combination of photographs (including one from the International Space Station), bathymetric data, and ASs data leads to the discovery of yet another source of internal waves in this area, produced during slackening tide by propagating lee waves that develop over a deep trench. We suggest that both the cross-channel circulation as well as the (solitary) internal waves may locally be of importance for the (re)distribution and transport of sediments and nutrients and may influence tidally averaged transports.

Responsible Editor: Jörg-Olaf Wolff

S. Groeskamp · J. J. Nauw · L. R. M. Maas (✉)
NIOZ Royal Netherlands Institute for Sea Research,
P.O. Box 59, 1790 AB, Den Burg, the Netherlands
e-mail: maas@nioz.nl

Keywords Estuarine circulation · Internal waves · Solitons · Tides

1 Introduction

1.1 Estuarine circulation

Because of the commercial and ecological value of estuaries, improving our understanding of their dynamics is of great importance. This has led to estuarine classification schemes (Hansen and Rattray 1966; Dyer 1973) and to overviews of estuarine dynamics (Neilson et al. 1989; MacCready and Geyer 2010). The most important characteristic of an estuary is the dilution of saline water with freshwater, leading to density gradients that drive estuarine circulation (Neilson et al. 1989). Pritchard (1952, 1954, 1956) found that the dynamics of the estuarine circulation that thus developed could be predicted with a tidally and cross-sectionally averaged linear model containing a balance between bottom friction, a pressure gradient term due to the along-estuarine surface slope, and a baroclinic pressure gradient. Analytical and numerical solutions of this model showed the flow to be sensitive to the choice of mixing parameterizations, but observations proved these predictions to be quite accurate (Geyer et al. 2000; MacCready 2004). Tidal and cross-sectional averaging performed in the linear Pritchard model resulted in the neglect of (nonlinear) intra-tidal processes, such as differential advection (Lerczak and Geyer 2004; Scully et al. 2009) and tidal straining (Simpson et al. 1990; Geyer et al. 2000) that contribute significantly to the net estuarine circulation. Also, tidal current and mixing asymmetries were ignored which might

Published online: 10 August 2011

dominate density-driven pressure gradients (Burchard and Baumert 1998). Other mechanisms that may contribute to net circulation in an estuary, not considered in the Pritchard model, are tidal rectification (Huijts et al. 2009), Ekman transport due to Coriolis force (Winant 2007), and other deflecting effects, such as due to channel curvature (Kalkwijk and Booij 1986; Buijsman and Ridderinkhof 2008; Huijts et al. 2009). Obviously, variability of freshwater discharge and wind exert an influence upon the net estuarine circulation as well. The range of frequencies of the different forcing mechanisms mentioned guarantees that estuaries never reach steady state (Bowden and Gilligan 1971), so that any particular observation is hard to relate to one particular physical cause (Souza and James 1996; Scully and Friedrichs 2007; Buijsman and Ridderinkhof 2008).

The above description of the state of knowledge on estuarine circulation contains a paradox: A classical linear approach works seemingly well for the prediction of tidally averaged estuarine circulation while many (intra)tidal, often nonlinear processes, that have proven to be of great importance for net estuarine circulation have been neglected (MacCready and Geyer 2010). This paradox is resolved by recognizing that Pritchard's description of the sub-tidal estuarine circulation rests on the use of properly chosen bulk parameters. Subsequent, more refined studies rationalize these choices by unraveling underlying processes. In the present paper, observational evidence is provided for the existence of yet another such factor potentially important for the exchange of water, mixing, and estuarine circulation, namely the (periodic) temporal presence of stratification leading to the sudden appearance of strong intra-tidal estuarine circulation and internal waves (IWs), even in a highly energetic environment. The IWs are (nonlinear) events that, in certain estuaries, might contribute to mixing as much as bottom friction does (Wang 2006). Stacey et al. (2001) explain the suddenly appearing temporal "pulses" of estuarine circulation within a tidal cycle using a threshold mechanism in which damping of turbulent mixing due to stratification leads to a positive feedback increasing the strength of stratification and associated vertically sheared currents. They argue that such mechanism is of great influence for net transports such that an accurate representation in sediment models is crucial. In this paper, we present supporting evidence for the existence of such pulses and argue that the strength of the measured currents associated with the intra-tidal estuarine circulation and IWs suggest that these might indeed influence the sub-tidal estuarine circulation.

1.2 Internal waves

IWs are generated in a vertically stratified estuary by flow over topography, by decelerating river plumes advancing in a stratified sea, or by (near) resonance in transcritical flow. A strong tidal flow (velocity $|u| >$ IW phase speed $|c|$) results in a baroclinic pressure gradient building a stationary, deepening lee wave. The relaxation of the baroclinic pressure gradient causes up- and down-current propagating IWs. In up-current direction, the IWs are arrested by the barotropic tide when $|c| < |u|$. As soon as $|c| > |u|$, a solitary internal wave (SIW) train may develop, traveling with a Doppler-shifted speed that is approximately $|c| - |u|$. This mechanism was first proposed by Maxworthy (1979), using laboratory experiments, and was verified in Knight Inlet, using echo soundings (Farmer and Smith 1980; Farmer and Armi 1999). Wang (2006) modeled this generation mechanism accurately.

Pressure differences building up at a front (or river plume) moving into a stratified ambient may also be relaxed by propagating SIWs, when the phase speed of the waves becomes larger than the speed at which the front advances. This mechanism leads to SIWs propagating in the same direction as the front as observed for Columbia River plume front (Nash and Moum 2005; Pan and Jay 2008) and for the tidal intrusion front in Sequim bay (Marmorino and Smith 2007).

In a stratified and vertically sheared horizontal flow, internal waves may also develop as instabilities when the flow is near-resonance ($u \pm c = 0$), the so-called transcritical flow regime. These internal waves are often prompted by depth or width changes of the tidal channel. Here the background velocity and linear long internal wave speed need both to be corrected for the shear current. Both up- and downstream traveling SIWs can be generated during the acceleration or deceleration phase of the tide. Da Silva and Helfrich (2008) have observed such generation of SIWs during both the accelerating and decelerating phase of the tide in Race Point Channel. Bogucki et al. (1997) found resonantly generated SIWs in a stratified bottom layer in the California shelf, which significantly contributed to vertical mixing. Neither the resonant nor frontal generation mechanisms necessarily need bottom topography to generate SIWs, but some geometric constriction usually acts as incipient point of unstable growth. Once SIWs are present in an estuary, they may transport sediments and nutrients and can cause mixing of different water masses, leading to a fresh supply of silt and nutrients (Sandstrom and Elliott 1984). As a result, IWs

can be of importance for biological activity in an area and are therefore studied in detail here.

The establishment of vertical stratification supporting IWs is delicate because estuaries may rapidly swap between vertically well-mixed and stratified conditions due to a constant competition between discharge leading to stratification and tidal and wind-induced mixing processes that homogenize the fluid vertically (Simpson et al. 1990; Souza and James 1996; De Boer et al. 2006). The importance of IWs for the dynamics of estuaries has been acknowledged, based on several observations. For example, Dyer (1982) found salinity fluctuations caused by IWs with periods of 4–8 min with wavelengths of 60–120 m in the Southampton Water. Using an echo sounder, IWs with amplitudes of a few meters and periods in the order of a minute were observed in the Fraser estuary in British Colombia during ebb currents in periods of stratification, alternated by periods of strong mixing (Geyer and Smith 1987). An echo sounder also revealed evidence of upstream-traveling IWs in the Tees estuary (New et al. 1987). Trains of short period (5 min) IWs of decreasing amplitude and unknown source were observed in the Huanghe Delta Front as well (Wright et al. 1986).

Recently, surface manifestations of what appear to be SIWs were repeatedly spotted in Marsdiep estuarine tidal channel (Section 2), where they take the shape of elongated bands of deviant surface roughness, extending in cross-channel direction (Fig. 1). This suggests that SIWs might exist also in Marsdiep channel (Hughes and Grant 1978; Osborne and Burch 1980; Farmer and Armi 1999), despite the fact that mixing due to wind and tidal currents is often so vigorous that the water is usually vertically well-mixed (Postma 1954; Buijsman and Ridderinkhof 2008). A photograph of the same area, taken on another day by an astronaut from the International Space Station (ISS; Fig. 2), shows the same typical surface manifestation as one would expect from SIWs when observing from above (Apel et al. 1975; Fu and Holt 1984; Cresswell et al. 1996; Nash and Moum 2005; da Silva and Helfrich 2008), supporting the idea of regular occurrences of IWs in Marsdiep channel. In addition, captains of a ferry crossing the Marsdiep 16 times a day have repeatedly seen this pattern in the water, with estimated crest-to-crest length of 50–100 m and crest width of a few 100 m, and also claimed to have sensed its presence with the ship in the form of long-period swell. The main purpose of the present study is to show evidence of a new unexpected generation site for SIWs (Marsdiep channel). SIWs are triggered during slackening tide, either as instability of the shear flow that develops or by relaxation of a lee wave forced by tidal flow over topography. This warrants further study because of their potential importance for the dynamics in this area. It also supports the idea that IWs might be more pronounced in highly energetic estuaries than recently expected and should therefore be included in model studies as an important factor for mixing and as a contributor to intra-tidal velocities and tidally averaged circulation.

In this paper, 20 days of high-frequency acoustic Doppler current profiler (ADCP) measurements in an estuarine tidal channel is presented. These observations show the presence of tidal currents, the effects of

Fig. 1 Photographs of Marsdiep inlet taken from the ferry, on different dates, of the region indicated by "A" in Fig. 2. A few long bands of "rougher" water are seen. These might be the surface manifestation of internal solitons. The *left picture* (by S. Groeskamp) during late ebb and the *right picture* (by C. Maas) during flood

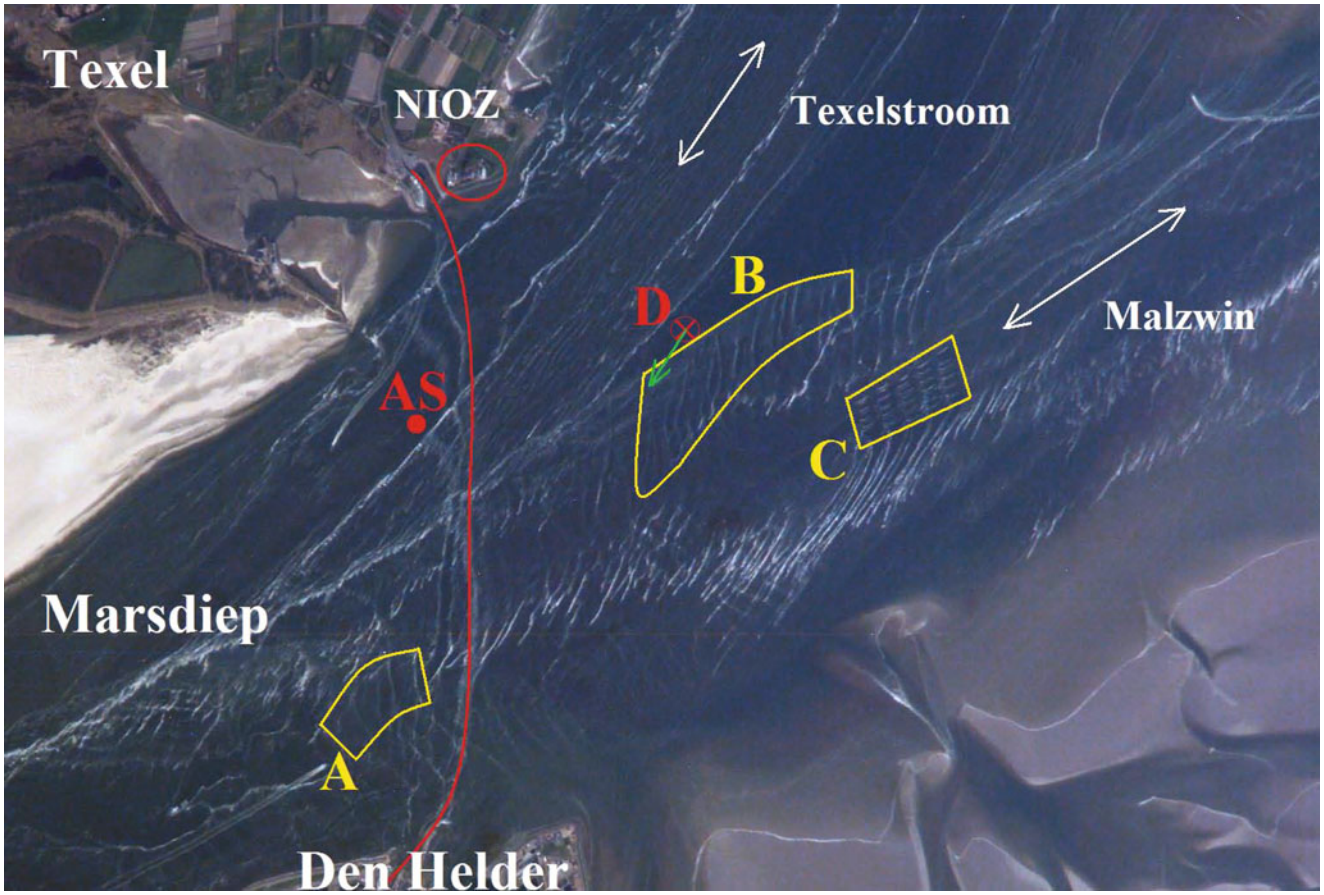

Fig. 2 A photograph of the Marsdiep taken by an astronaut onboard ISS on 1 May 2007 during late ebb. More details and an indication of the scale of the location are described in Section 2. The *red circle* indicates the location of the NIOZ. The *red cross* marks the location of the deployment (*D*), and the *filled red dot* marks the location of anchor stations (*AS*) taken by RV Navicula. The *green arrow* shows the propagation direction of the first soliton of ebb slack 22 (Section 6.3). The *white arrows* denote the direction of the two main currents. The *red line* is the approximate ferry track. Regions *A* and *B*, marked with *yellow*, indicate the locations (near the Ferry and near the deployment), where the surface expressions of SIWs might be seen. The area *C*, also marked *yellow*, is an artificial structure to breed mussels (musselseed installation)

curvature and of frictional and Coriolis forces, and, more importantly, the presence of intra-tidal estuarine circulation and up-stream traveling SIWs. To our knowledge, such accurate moored recordings of SIWs in a highly energetic estuary, characterized by strong temporal and spatial variability of its stratification and tidal currents, have not been presented before. It demonstrates the apparent inevitability of IWs in stratified regions accompanied by either current shear or uneven bottom topography. After a discussion of the study area in Section 2 and the data collection and processing methods in Section 3, the measurements will be analyzed in Section 4. Using harmonic analysis, the so-called coherent current is obtained that consists of persistent motions at tidal frequencies. Subtracting the coherent current from the original measurements leaves the "incoherent" current, which is forced by frequencies other than tidal and usually contains all baroclinic flow components. Definite proof of vertical stratification in Marsdiep that may manifest IWs is given in Section 5. The observed circulation patterns and IWs in the incoherent current are presented in Section 6. The paper ends with a discussion and conclusion of the results in Section 7.

2 Study area

The Wadden Sea (Fig. 3) is an inland sea in western Europe stretching from the Netherlands to Denmark. Its unique ecology offers one of the most precious natural habitats in this area. The Wadden Sea is connected to the North Sea through tidal inlets between barrier islands separated from one another by vast tidal flats.

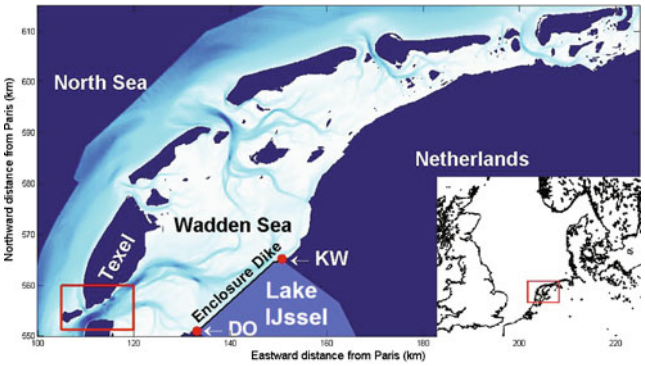

(a) Western Dutch Wadden Sea

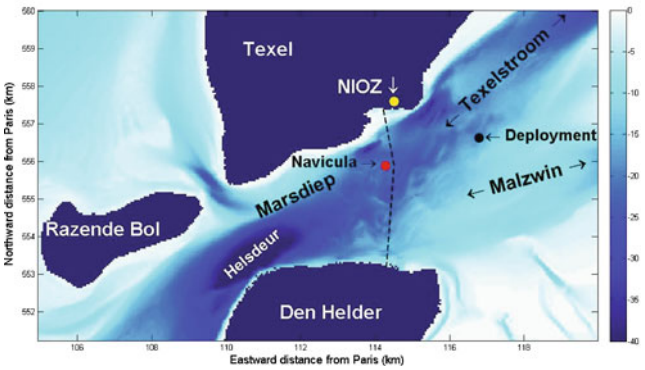

(b) Marsdiep Channel

Fig. 3 Bathymetry of the Wadden Sea (**a**) and Marsdiep (**b**) (color scale in meters), with a more global *inset* in the *lower right corner* of **a**. The *red square* in **a** shows the area enlarged in **b**. *Dark blue* indicates land, tidal flats, or an area where no data are available, as in the *upper left area* in **a**. Lake IJssel is colored *light blue*; its sluices are located at Kornwerderzand (*KW*) and Den Oever (*DO*). In the Marsdiep, the locations of Malzwin and Texelstroom currents, NIOZ Institute, deployment site, and Navicula ASs are shown together with the track of the ferry (*dashed line*). Helsdeur (a 50-m pit from which SIWs propagate eastward) is clearly identified by its *dark color*

The Marsdiep channel is located in the northwest of the Netherlands, between Den Helder and the island of Texel. Marsdiep channel (8 km long and 3.5–4.5 km wide) is one of the largest estuarine tidal inlets through which tidal exchange of water between North Sea and Wadden Sea takes place and therefore has an important role in determining the state of the Wadden Sea. As a result, many studies have been performed on Marsdiep channel and surrounding areas of which details are shown in Fig. 3.

Postma (1954), using observations on its hydrography and chemistry, showed that the tides in the Marsdiep, due to bottom frictional effects, are a combination of a progressive and standing wave and recognized tides as the most important physical process in the Wadden Sea. The latter was verified by Zimmerman (1976a, b) using salinity measurements. With a numerical model, Ridderinkhof (1988a) calculated a mean flow out of the Marsdiep for the Western Dutch Wadden Sea. Ridderinkhof (1988b) used an analytical model with which he could determine which terms are responsible for the net flow out of the Marsdiep. Using an extended version of the analytical model, in combination with long term (4 years of) ferry observations, Buijsman and Ridderinkhof (2007b) verified and accurately quantified this outflow. The currents in the Marsdiep are dominated by the semi-diurnal tide and can reach values of 1.8 m s^{-1} during spring tide (Buijsman and Ridderinkhof 2007a). As a result, deflecting effects due to channel curvature and Coriolis force are significant, leading to cross-stream circulation (Buijsman and Ridderinkhof 2008). Wind is a variable but common feature in Marsdiep area and may reach force 8 or higher on the Beaufort scale, several times per year.

The Marsdiep is diluted with freshwater entering from the Wadden Sea via Texelstroom and Malzwin channels, originating from discharge of Lake IJssel sluices at Den Oever and Kornwerderzand (Fig. 3a). Strong mixing processes in Marsdiep and Wadden Sea reduce vertical stratification. Cross-channel density gradients were observed in Marsdiep, with fresher water to the south, attributed to higher discharge, and shorter transit times of the Malzwin current compared to Texelstroom (Zimmerman 1976a, b). Buijsman and Ridderinkhof (2008) quantified the effects of the cross-channel density gradient on the cross-channel circulation pattern and their conductivity, temperature, depth (CTD) measurements provided the first indications of possibly periodic vertical stratification in Marsdiep. Measurements presented in the present paper confirm the alternating presence of vertically well-mixed and stratified conditions in Marsdiep, giving definite proof of the existence of strong temporal vertical stratification and horizontal density fronts.

3 Data collection and processing

From 9 April 2009 until 29 April 2009, almost 20 days of data is collected with a downward looking 1,200-kHz RDI Workhorse Rio Grande ADCP, mounted in a syntactic elliptical buoy at 52°59′43 N and 4°49′05 E, located in the southern part of the Texelstroom current and northern part of the Malzwin current at position D, the cross in Fig. 2, where the water is approximately 18 m deep. Velocities in the water column were sampled from 1.5 m beneath the surface to the bottom with a vertical resolution (binsize) of 0.5 m, a sampling period of 3 s, and a standard deviation of 2.32 cm s^{-1}.

Extreme pitch and roll events, software errors, and connection failures resulted in data gaps of one to 20 subsequent profiles of 6–60 s duration. The missing vertical profiles of all retrieved variables are linearly interpolated to restore a 3-s sampling interval. Several larger gaps, order 1–60 min and a total of 4.7% of data set, are considered lost. The acoustic backscatter intensity (ABI), given in counts, is recalculated to decibels and corrected for attenuation and geometrical spreading (Deines 1999). The eastward (u), northward (v), and vertical (w) velocity data are corrected for pitch, roll, and vertical or horizontal displacements, using motion relative to the bottom as reference. Consequently, velocity profiles are rejected when less than three beams were able to detect the bottom. Due to ADCP side lobe effects, the first bin above the bottom is rejected. Horizontal speeds ($= \sqrt{u^2 + v^2}$) larger than 2 m s^{-1} and absolute vertical velocities exceeding 0.4 m s^{-1} are considered physically unrealistic and are rejected in both the u, v, and w measurements. To remove spikes and reduce small current fluctuations due to surface (wind) waves, the result is filtered by a running mean over 21 points ($= 63$ s). Finally, defining the along-stream direction α by the maximum flow direction of the two depth bins closest to the surface based on currents of magnitude larger than 1 m s^{-1}, u, and v are rotated to along-stream ($\tilde{u} = u\cos\alpha + v\sin\alpha$) and cross-stream ($\tilde{v} = v\cos\alpha - u\sin\alpha$) velocity profiles. This results in an angle $\alpha = 62.6°$ T (degrees true north, oriented clockwise relative to north), in between the orientation of the Texelstroom and Malzwin channels (Figs. 2 and 3). As a result, a positive along-stream velocity is directed into the Wadden Sea (flood) and vice versa. A positive cross-stream velocity is, more or less, directed toward Texel, i.e., approximately toward the north. Vertical upward velocity is positive.

4 Coherent current

The coherent current is defined as motions that are forced at tidal frequencies and that persist over the whole duration of the time series. The incoherent current, typically incorporating the much more variable baroclinic flow components, represents the original measurements from which the coherent current is subtracted. This method of separating the measured data allows us to obtain an intra-tidal resolution of fast processes contributing to the estuarine circulation. A good approximation for the coherent current is obtained by fitting amplitudes and phases to tidal components present in the measurements, using least squares harmonic analysis (LSHA; Emery and Thompson 2001; Buijsman and Ridderinkhof 2007a). Following Emery and Thomson (2001), the measurements are described by:

$$U_i = \underbrace{\bar{U} + \left[U_0 + \sum_{j=1}^{N} U_j \cos(\omega_j t_i - \phi_j) \right]}_{\text{Coherent Current}} + \hat{U}_i \qquad (1)$$

Here U_i represents a direct measurement and $\bar{U} = \frac{1}{I}\sum_i^I U_i$ is the average over the time series containing I measurements at times t_i, such that $i \in (1, I)$. The LSHA fit is represented by the part within brackets, with U_0 its tidal average, U_j and ϕ_j the amplitudes and phases at frequencies ω_j, and N the amount of tidal frequencies used. Finally, $\hat{U}_i$ is the zero-mean residual or *incoherent current* which are motions forced at all other frequencies. Before applying the LSHA, the average ($\bar{U}$) is subtracted from the measurements to reduce round-off errors. If the average is subtracted before applying the LSHA, nonzero U_0 results due to incomplete tidal cycles over the duration of the time series. The physical mean current over the measured period is given by $U_n = U_0 + \bar{U}$.

The tidal frequencies (ω_j) used for the LSHA need to satisfy three criteria. First, the period of the smallest (fundamental) frequency (T_f) that can be resolved is smaller than or equal to the duration of the time series (T) leading to $T_\mathrm{f} \leq T = 19.8$ days. Second, the period (T_N) of the largest (Nyquist) frequency that can be observed is equal to twice the sampling interval leading to $T_\mathrm{N} = 2\Delta t = 6$ s. Third, two adjacent frequencies can only be resolved if the reciprocal of the frequency difference is smaller than or equal to the duration of the time series leading to $\frac{1}{\Delta f} \leq T$ (Rayleigh criterion). Here Δf is the difference between two adjacent frequencies used for the LSHA. The criteria above are applied to the 25 most dominant and annual, semi-annual, monthly, and fortnightly frequencies for the sea level height variation in Marsdiep (Buijsman and Ridderinkhof 2007a). A total of 14 out of the 25 most dominant frequencies satisfy the criteria with which a LSHA is performed on time series of along and cross-stream velocity at each available depth level. The percentage of explained variance, for the along (cross) stream time series, varies between 83.0% and 96.4% (26.4% and 85.6%) with an average overall depths of 95.6% (71.0%). The lowest values are located close to the bottom and near the surface. There, bottom frictional or wind stresses cause an increase of incoherent processes and therefore a decrease of the importance of tidally forced processes.

5 Vertical stratification in Marsdiep

For IWs to exist in Marsdiep, vertical stratification is necessary. Only one previous publication indicates possible periodic vertical stratification in Marsdiep (Buijsman and Ridderinkhof 2008). Meanwhile, 21 13-h anchor stations (ASs) with R.V. Navicula acquired measurements of vertical profiles of velocity, ABI, and density throughout the past 6 years, the results of some of which will be discussed here. The location is situated in the Texelstroom, approximately 2 km west of the deployment (see Figs. 2 and 3b). From the AS data, a relation between stratification and velocity can be obtained. The measurements are obtained using a downward looking Nortek 1.0 MHz ADCP, mounted at the side of the ship, and the water column is measured from 2.51 m beneath the surface to the bottom, with a vertical resolution of 0.99 m and a frequency of 1 Hz.

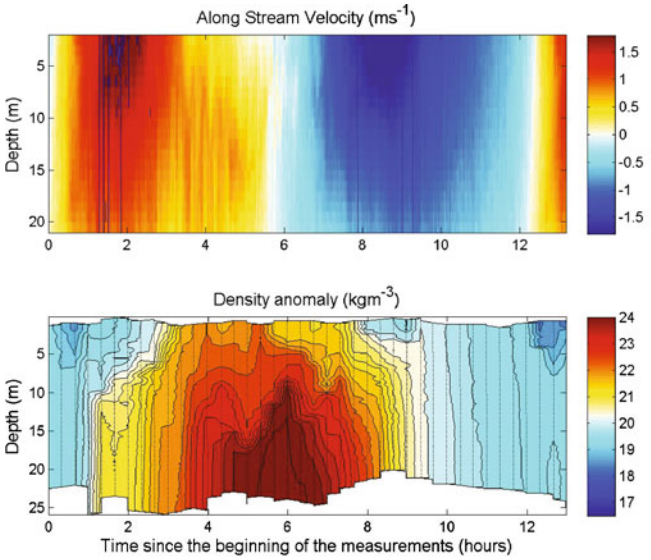

(a) AS 49, 06-04-2007

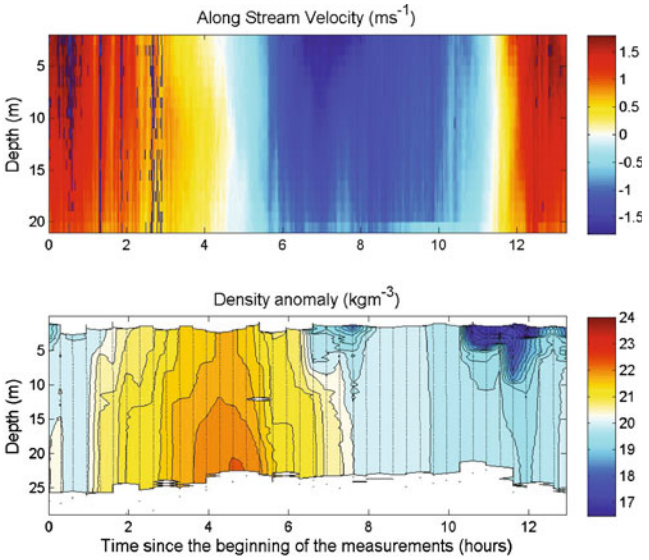

(b) AS 51, 28-09-2007

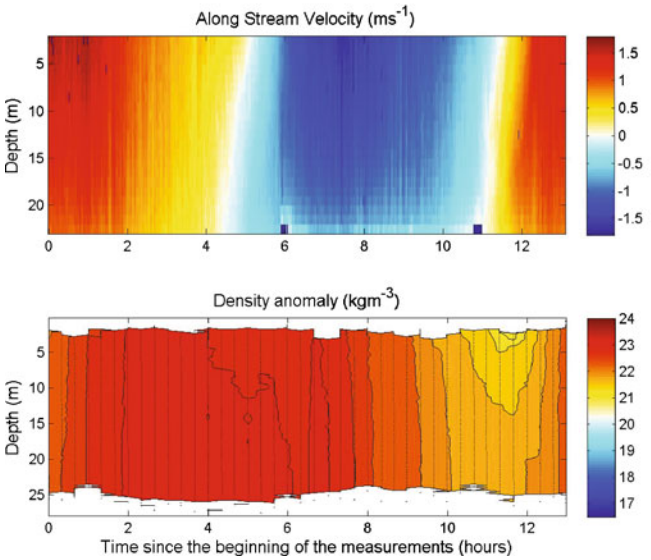

(c) AS 54, 20-06-2008

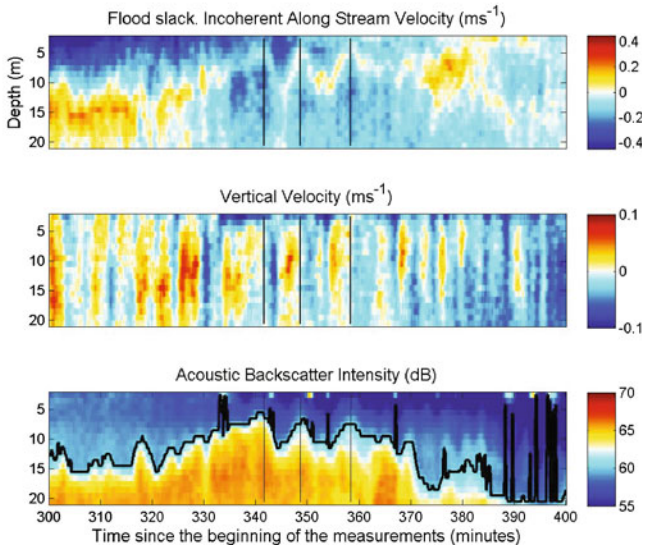

(d) AS 49 Slack, 06-04-2007

Fig. 4 Along-stream velocity (*top*) and density minus 1,000 kg m^{-3} (*bottom*) for AS49 (**a**), AS51 (**b**), and AS54 (**c**), obtained by RV Navicula at location shown in Fig. 3b. Positive, *red* (negative, *blue*) along-stream values indicate a flood (ebb) current into (out of) the Wadden Sea. The *vertical dashed lines* indicate CTD downcasts. The *upper*, *middle*, and *lower* panels of **d** show, respectively, the along-stream incoherent velocity, vertical velocity, and ABI plus interface (*black line*) of flood slack AS49. *Black vertical lines* indicate positions of wave crests indicating possible IW motion

The accuracy of the velocity measurements is approximately 1% of its magnitude. Every 20 min, a CTD with Seabird sensors was lowered from the surface to the bottom. With an accuracy of 0.004°C, 0.005 psu, and a vertical resolution of 0.05 m, it measures depth and density (from pressure, temperature, and conductivity).

From the 21 ASs, three examples are selected that show typical events occurring during a tidal cycle in Marsdiep. After rotating the horizontal velocity to along and cross-stream velocity, Fig. 4a–c shows the measured along-stream velocity (upper panels) and density (lower panels) of AS49 (calm wind, Bft 2 on 6 April 2007), AS51 (28 September 2007, stormy to moderate wind), and AS54 (moderate wind, Bft 3-6 on 20 June 2008), respectively. The density is displayed on a scale between 16.5 and 24 kg m^{-3} at 0.25 kg m^{-3} interval lines. Positive, red (negative, blue) along-stream values indicate transport into (out of) the Marsdiep, i.e., flood (ebb) currents. From the ASs in general (and Fig. 4 specifically), one can conclude that tidal mixing due to strong flood and ebb currents leads to a vertically well-mixed water column. When tidal velocities decrease, tidal mixing weakens and stratification sometimes develops. As AS54 shows, which is well-mixed during the complete tidal cycle, this is not always the case. If stratification develops, this is either during flood slack (low velocity during the transition from flood to ebb), related with the intrusion of relatively saline North Sea water over the bottom (as in AS49 for 4 h $< t <$ 7 h), or during ebb slack, when freshwater discharge from Lake IJssel leads to a fresh surface layer (as in AS51 for 10 h $< t <$ 12 h). Between slacks, vertically well-mixed conditions are always reached, such that vertical stratification needs to reestablish each slack. This leads to variability in the strength of stratification depending on, for example, the phase of the spring neap cycle (Pritchard 1989; Walters 1989; Chant 2002; De Boer et al. 2006), volume of freshwater discharge, and stirring by local windstress.

In several ASs, indications of motions related with IWs are found during flood slack, very likely related with the stratification caused by the intrusion of saline North Sea water over the bottom. The most clear example is found during the flood slack of AS49. To emphasize the baroclinic component, in the upper panel of Fig. 4d, the coherent current is subtracted from the measurements using the LSHA method as described in Section 4. Also the vertical velocity and ABI of that flood slack are shown in the other two panels of Fig. 4d. The ABI is accompanied by a black line representing the "interface." The ABI interface is the depth at which the ABI is equal to its average *over the duration shown*. During periods of low tidal velocities (around slack), we may assume that turbulence and associated mixing is reduced and restricted to the bottom boundary layer. The ABI interface is then an indication of the depth of the interface between the turbid bottom layer and fresher, less turbid surface layer. A wave pattern is visible in the vertical shear of the along-stream incoherent velocity, starting at approximately $t = 340$ min. Vertical black lines indicate when vertical motion is zero while waves in the ABI and along-stream current reach extreme values. This indicates a 90° phase difference between motions of the interface and vertical velocity, indicative of propagating interfacial waves (Neumann and Pierson 1966; Defant 1961). Note the wave's large amplitude and relatively long period, which excludes forcing by high-frequency turbulence or surface waves. The AS data thus proof that vertical and horizontal stratification is present in Marsdiep and indicates the manifestation of interfacial IWs. In combination with three photographs of surface manifestation of IWs (Figs. 1 and 2), we now have good reasons to expect that also the deployment data will manifest IWs.

6 Incoherent current

Buijsman and Ridderinkhof (2008) derived a conceptual model of the cross-stream circulation patterns in Marsdiep, covering several parts of the tidal cycle during well-mixed and stratified conditions, using an analytical model supported by measurements. Measurements presented here show the presence of IWs and relatively strong cross-channel circulation patterns before and during ebb slack, which are partly explained using the same mechanisms as proposed by Buijsman and Ridderinkhof (2008). In the remainder of this article, we will therefore discuss the tidal phase between maximal ebb and flood velocities, including ebb slack. In almost 20 days of measurements, 38 ebb slacks are covered. Both the circulation patterns and IWs influence the ABI and thus the suspended matter, indicating their importance for distribution and transport of (dissolved) material. Using two examples of measured ebb slacks, the generally observed sequence of changing velocity patterns is explained.

6.1 Positive lateral shear

The first example is shown in Fig. 5. The left column shows three panels with measurements made during the first ebb slack. The along-stream velocity (upper panel) shows a phase lag and increasing values from bottom to surface, as expected for a barotropic tidal

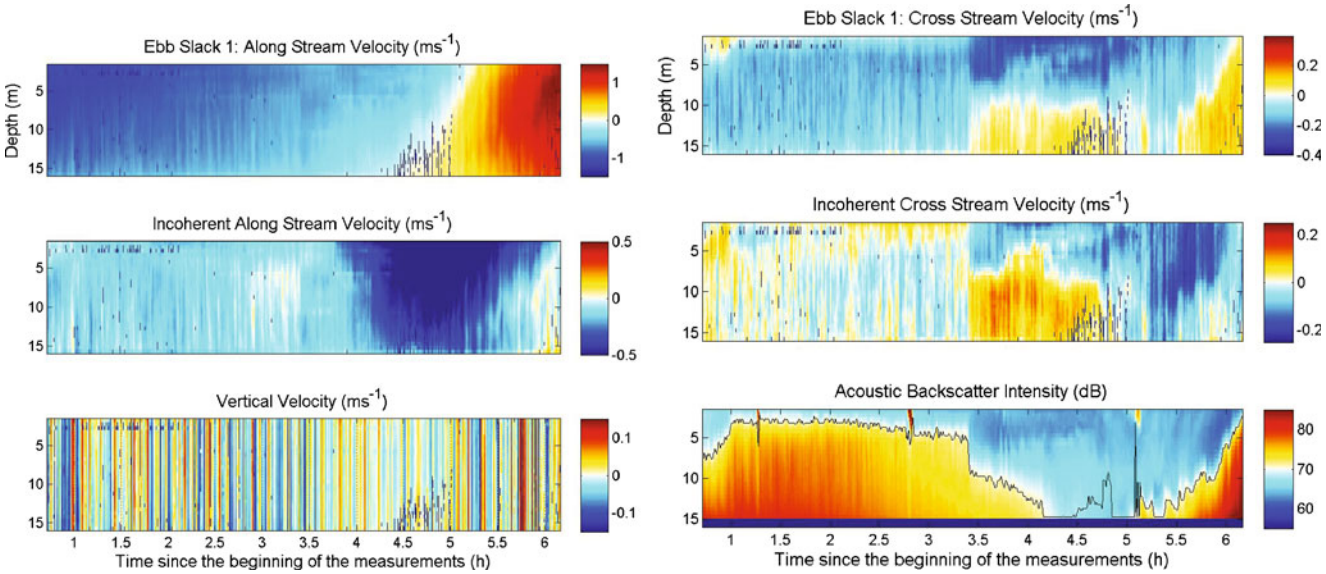

Fig. 5 Ebb slack 1 (9 April 2009). The *left column* shows three figures which are, from *top* to *bottom*, the along-stream measurements, incoherent along-stream velocity, and vertical velocity. The velocity color scale (meters per second), different in each panel, is given to the *right* of each panel. The sign refers to the rotated coordinate frame (positive into Wadden Sea and toward Texel, respectively). The *right column* shows, from *top* to *bottom*, the cross-stream measurements, incoherent cross-stream velocity, and ABI with interface (*black line*). In the latter, the last few bins are removed because very high values due to bottom interference sometimes leads to non-physical results influencing the calculated interface

current subject to bottom friction (Prandle 1982; Maas and Van Haren 1987; De Boer et al. 2006). Strong shear, other than due to bottom friction, is absent in the incoherent along-stream velocity field (middle panel). Shear due to baroclinic effects, as for example horizontal density gradients, is not present. If it were, it would have been pronounced in the along-stream incoherent signal because it is not coherent with tidal frequencies and would thus not have been subtracted along with the bottom friction effects.

By contrast, in cross-stream direction, shear is observed in both the measured and incoherent currents (top and middle panel of right column). Initially, during late ebb ($t < 3.4$ h), an almost vertically uniform southerly (cross-channel) current is measured. This is not visible in the incoherent cross-stream velocity and must therefore result from a coherent process. Recalculating the LSHA horizontal velocity amplitudes and phases into rotary components (Prandle 1982; Maas and Van Haren 1987), it is found that the anti-clockwise velocity amplitude is larger than the clockwise velocity amplitude over the whole water column. This leads to an anti-clockwise rotating tidal ellipse in the *horizontal* plane in Marsdiep at the location of the deployment, which is also observed by Buijsman and Ridderinkhof (2007a). In an anti-clockwise rotating tidal ellipse, between maximal ebb and ebb slack, the current veers in negative cross-stream direction. Note that deflection of the current due to Coriolis force would lead to a clockwise rotating ellipse; therefore, other (possibly nonlinear) deflecting effects must be responsible for the southward directed cross-channel flow. Following Buijsman and Ridderinkhof (2008), we suspect that channel curvature is the most likely cause.

Suddenly, at $t = 3.4$ h, the vertically uniform structure of the measured and incoherent cross-stream current changes into positive lateral shear (PLS), called so because the associated vorticity in the y–z plane is positive when looking in positive x (flood) direction. This change appears within 2 min, lasts approximately 90 min, and is accompanied by a simultaneous drop in the ABI interface. Before $t = 3.4$ h, suspended matter is distributed throughout the whole water column while at $t = 3.4$ h; when the PLS occurs, the water column is restructured into a bottom and surface layer. The change is strong and quick, suggesting that sudden local settling of suspended matter is unlikely. It is important to recognize that the ABI interface drops to the same depth as that of the interface between the two layers of the PLS, which suggests that cross-channel current and not the stronger along-stream current dominates the distribution of suspended matter in this phase of the tidal cycle in Marsdiep.

The rapid change to PLS is measured during 33 of the 38 ebb slacks, and most are accompanied by the ABI interface drop. Since only stationary measurements

are available, it is not known exactly which processes lead to the change at $t = 3.4$ h. Slackening of the tide, leading to reduced turbulent mixing, leaves a baroclinic pressure gradient unchecked, possibly giving rise to the onset of the sheared gravity current (Stacey et al. 2001). The orientation of the circulation measured by the deployment would then suggest an along-channel freshwater front advected from the north to the south. Previous measurements did not have a sufficient space and time resolution that such changes could be measured. On the contrary, fresher water is commonly found *south* of Marsdiep channel (Buijsman and Ridderinkhof 2008). Nonetheless, if the Texelstroom current is horizontally sheared, differential advection may *locally* lead to transverse density gradients that subsequently produce cross-currents and vertical stratification (Burchard et al. 2011). At the deployment site, south of the Texelstroom (during ebb current), the shear associated with such stratification would have the same orientation as the measured shear. Therefore, during the ebb phase of the tidal cycle, differential advection of the Texelstroom can lead to local cross-channel and vertical stratification which dampens turbulent mixing, leading to a positive feedback in which stratification and associated shear currents instantly develop (Stacey et al. 2001).

6.2 Negative lateral shear

A different kind of suddenly appearing shear pattern is observed in the 25th ebb slack, shown in Fig. 6. In this ebb slack, the PLS with ABI interface drop is observed at $t \approx 300.6$ h and lasts for approximately 80 min. Quite abrupt, at $t \approx 301.8$ h (see right panel), negative lateral shear (NLS) develops that lasts 25 min and affects the along- and cross-stream incoherent velocities and cross-stream measurements. At the same time, a second drop of the ABI interface is observed accompanied by strong down-welling. The down-welling is oftentimes accompanied by increased ABI values at the surface due to assimilation of material in what appears to be a convergence zone.

The NLS is observed in 28 out of the 38 ebb slacks in the incoherent cross-stream velocity. It varies in duration (20–30 min) and strength and appears suddenly. The NLS is more (or only) pronounced in the incoherent current, indicating that it is a strong incoherent process, such that predictable processes as deflection of the ebb current due to curvature or Coriolis force are excluded as its cause. We suggest that the NLS is caused by an along-channel front south of the deployment, generated by the relatively fresh Malzwin outflow next to more saline Texelstroom outflow, leading to density-driven NLS which expands north, passing the deployment. This is illustrated in Fig. 7 and visible in Fig. 2 bounded by axial foam lines that indicate a convergence zone (an example of the associated down-welling is visible in the lower panel of Fig. 6 just before $t = 302$ h, indicated by blue colors). The variability of the strength and duration of the resulting NLS at the front is likely due to changing influences of wind, tidal mixing, and discharge. At $t \approx 302.3$ h, the NLS currents lead to the generation of SIWs. This will be described in more detail in Section 6.3.

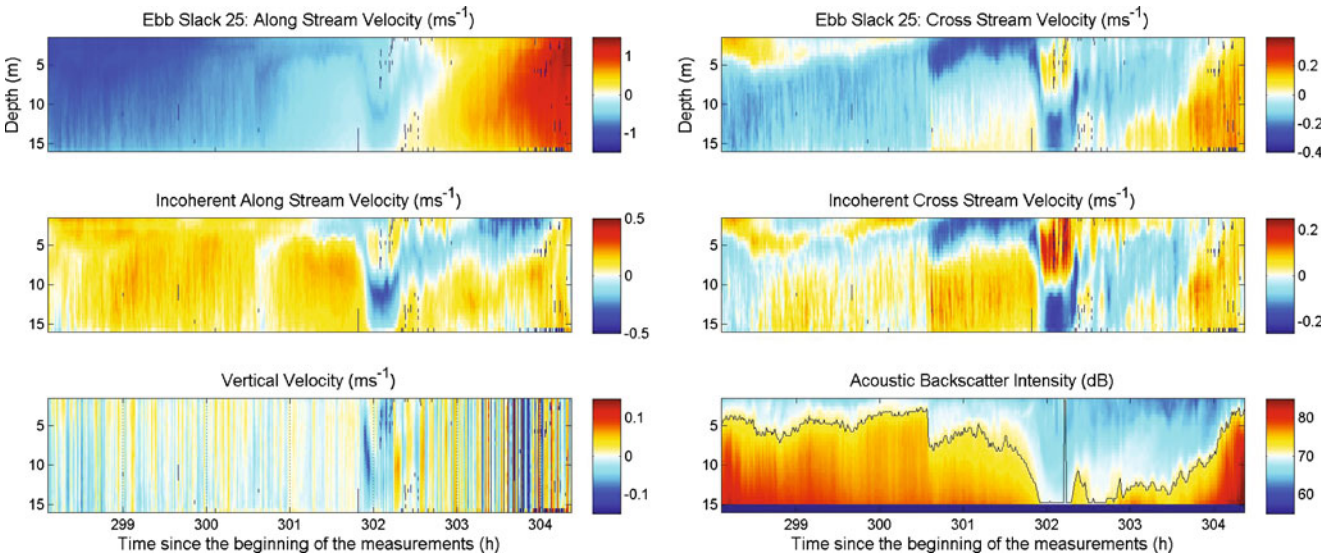

Fig. 6 As Fig. 5 but for ebb slack 25 (21 April 2009)

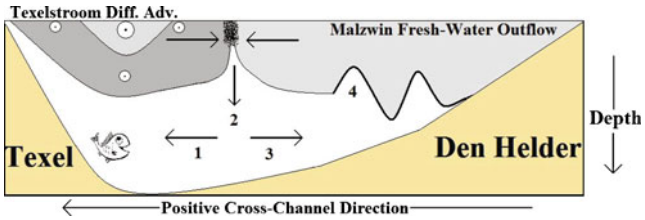

Fig. 7 Sketch of a cross section of Marsdiep inlet, looking into the Wadden Sea (i.e., positive x, or flood direction). The *dark* (*light*) *gray* indicates a saltier (fresher) water mass which show density fronts necessary to produce the observed shear patterns. Differential advection of the Texelstroom outflow (indicated with *circles*) leads to local stratification that causes PLS (*1*), followed by a convergence zone leading to downwelling (*2*) and the fresh Malzwin outflow that leads to NLS (*3*) and SIWs (*4*). At the convergence zone, foam (*black dots*) is observed near the surface

6.3 Solitary internal waves

This section shows that the density front that leads to the NLS also manifests propagating mode one SIWs. The vertical and incoherent cross-stream velocity fields of Fig. 6 carry some first indications of SIWs for $t >$ 302.3 h, but in an expanded time frame, Fig. 8 shows these waves much more clearly in the incoherent along- and cross-stream velocity, vertical velocity, and ABI of ebb slack 22. Positions indicated by vertical black lines show positions of troughs in the ABI and in the incoherent velocity profiles. Precisely at those instants, the vertical motion is zero and therefore exactly 90° out of phase with the ABI, again indicating typical manifestation of propagating interfacial waves. The vertical velocity has a uniform sign in the vertical and a maximum in the middle of the water column, which is a typical manifestation of mode one IWs (LeBlond and Mysak 1978; Defant 1961; Gerkema and Zimmerman 2008; Roberts 1975). The IWs are ordered in a wave train with decreasing amplitudes, one indication that the waves are nonlinear and therefore mode one SIWs (Ostrovsky and Stepanyants 1989; Gerkema and Zimmerman 2008).

The along-wave velocity beneath the interface of a SIW of elevation is in the direction of propagation (Defant 1961). During the first wave (in between the first two vertical lines of Fig. 8), the wave-induced current is in direction 209° T. This is determined using the tangent of the cross- and along-stream velocity of measurements beneath the wave crest. After rotating this single soliton in along-wave direction, as shown in Fig. 9 and indicated in Fig. 2 with a green arrow, the positive along-wave velocities beneath the interface thus indicate that the wave propagates in the same direction. One would expect the wave crests (or troughs) to be perpendicular to the direction of propagation. This is not the case for the solitons in Fig. 2. Apart from noting that the picture of Fig. 2 is taken on a different day than that during which the soliton of ebb slack 22 is measured, so that it is likely that the orientation of the Malzwin outflow has changed, the reason may

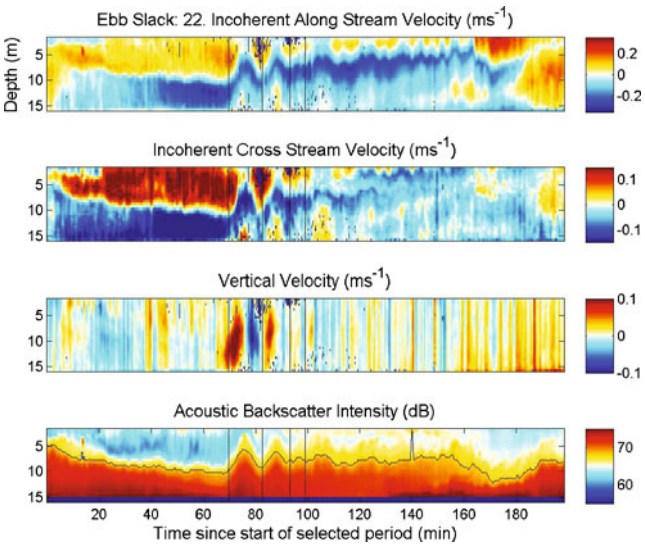

Fig. 8 Ebb slack 22 (20 April 2009). *Top* to *bottom*: incoherent along- and cross-stream velocity, the vertical velocity, and ABI with interface (*solid line*) when the depth average velocity is smaller than 0.75 m s^{-1} and larger than −0.5 m s^{-1}. *Vertical black lines* indicate locations of wave troughs with zero vertical velocity

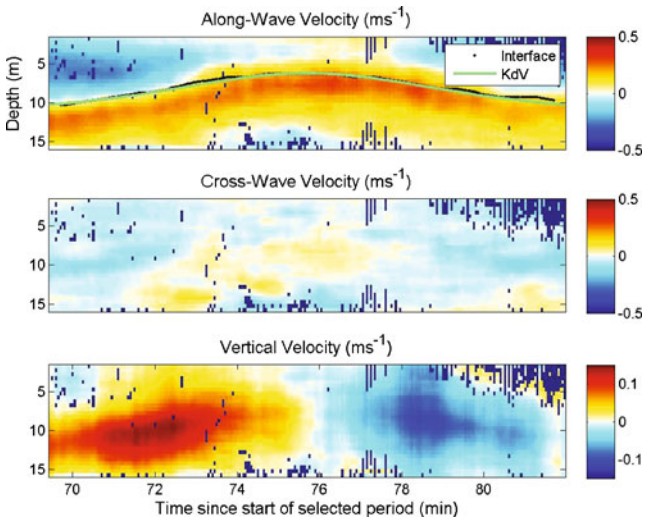

Fig. 9 Velocity components as a function of time (minutes) during the first soliton passage of ebb slack 22. Velocities are rotated into along- (209° T) and cross-wave direction (*first* and *second panel*). The vertical velocity is shown in the *third panel*. In the along-wave velocity (*first panel*), the calculated interface of the ABI (*black line*) and theoretical shape of KdV soliton (*green line*) are shown, lying nearly on top of each other

be that, first, shear in the Malzwin ebb current leads to clockwise rotation of the wave crests; second, that waves refract due to depth changes; and third, that layer thickness differences, again due to depth differences, may locally lead to phase speed differences (see Eq. 2 below). The presence of a nonzero, substantial vertically integrated volume flux in the propagation direction (Fig. 10) indicates nonlinear behavior and thus *solitary* internal waves (LeBlond and Mysak 1978; Pan and Jay 2008). In at least five of the 38 measured ebb slacks the NLS is followed by a train of mode one SIWs (see, for example, those on $t = 302.3$ h during ebb slack 25, Fig. 6).

Assuming Marsdiep has two layers of upper and lower layer depths h_1 and h_2, respectively, and the SIWs are long compared to the depth, then wave characteristics and the deviation of the layer interface from the unperturbed level (η) is given by a solution of the KdV equation (Ostrovsky and Stepanyants 1989):

$$\eta = \eta_0 \mathrm{sech}^2\left[\frac{x - Ct}{\Delta}\right]$$
$$C = c_0 + \frac{\eta_0 \alpha}{3}$$
$$\Delta = \sqrt{\frac{12\beta}{\alpha \eta_0}} \qquad (2)$$

where t is time (seconds), η_0 is the wave amplitude, C is the nonlinear phase speed, c_0 is the linear phase speed, Δ is the soliton half-width, α (per second) is the nonlinear coefficient, β (cubic meters per second)

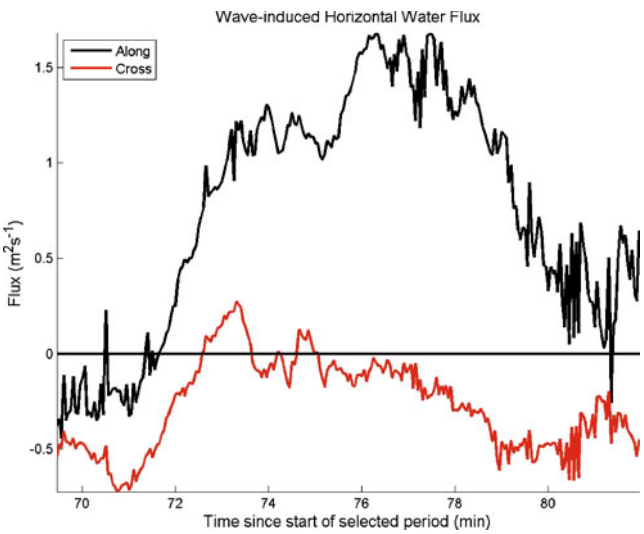

Fig. 10 The vertically integrated water flux in along- and cross-wave direction

is a measure for dispersion, and we take $x = 0$ as the fixed point at which our measurements are taken. To obtain an expression for c_0, α and β, we use the reduced gravity $g_0 = g\frac{\rho_2 - \rho_1}{\rho_2}$ in terms of densities of the surface (ρ_1) and bottom (ρ_2) layer (Gerkema and Zimmerman 2008). This results in $c_0 = \sqrt{g' \frac{h_1 h_2}{h_1 + h_2}}$, $\alpha = \frac{3c_0(h_1 - h_2)}{2h_1 h_2}$, and $\beta = c_0 \frac{h_1 h_2}{6}$. The depth of the interface, as visible in Fig. 9, yields thicknesses of the surface and bottom layer $h_1 = 9.5$ m and $h_2 = 8$ m. During the deployment, we had no direct density observations of the two layers. Assuming that those measured at the anchor station, Fig. 4b at $t = 11$ h, are typical for Malzwin freshwater outflow, we take $\rho_1 = 1{,}017$ kg m^{-3} for the surface layer and $\rho_2 = 1{,}020$ kg m^{-3} for the bottom layer during stratified conditions. This results in $c_0 = 0.35$ m s^{-1}, $\alpha = 0.01$ s^{-1} and $\beta = 4.49$ m^3 s^{-1}, which are kept constant for all five wave events that we study below. The individual waves and their amplitudes are manually determined from the measurements by carefully studying the relations between the horizontal and vertical velocities in combination with the ABI interface excursion. For each of the five ebb slacks in which SIWs are measured, the results are presented in Table 1 together with the duration of the NLS, the observed amount of waves, and the manually obtained and theoretically calculated wave period. The value for C is always approximately 0.36 m s^{-1} and thus not shown.

In general, the SIWs are ordered in wave trains consisting of two to six waves in which subsequent waves mainly show decreasing amplitudes in a range between 1.5 and 5 m. The computed wavelengths (ranging between 91 and 117 m) and periods (ranging between 172 and 325 s) increase with decreasing amplitude and seem to be in a realistic range. The assumption of long waves is correct because $h_1 + h_2 \ll \lambda$. In Fig. 9, the first wave of ebb slack 22 is used for comparison of the expected theoretical elevation of the interface due to a SIW (η) with the ABI interface using $\eta_0 = 5$ m. It shows a great resemblance and thus confirms that the measured waves are solitons.

However, the measured and computed periods are not consistent. Why is this, and does it tell us which generation mechanism is responsible for the SIWs? The measured periods are longer, which can only be achieved if the waves propagate with a speed C against the barotropic background current u, such that the net speed is less and thus the soliton period longer than that calculated using C. The propagation direction of the wave in Fig. 9 (209° T) is approximately the same as that of the temporal background current (211° T), determined using the *coherent* current during the first wave. This leads to the assumption that $|u| > |c|$. Therefore,

Table 1 SIW characteristics for several measured ebb slacks

Ebb slack #	15	21	22	25	38
Duration NLS (min)	63	71	61	23	21
# waves	3	2	3	4	6
η_0 (m)	2.5–2	3.5–3	5–2	4–2	4–1.5
$\lambda = 2\Delta$ (m)	91–101	77–83	64–101	71–101	71–117
$T = \frac{\lambda}{C}$ (s)	251–279	210–227	172–279	195–279	195–325
T_m (s)	750–800	900–1,100	350–775	330–600	225–775

From top to bottom, the rows give the duration of the NLS, the minimum amount of observed SIWs, the amplitude range (η_0), wave length range (λ), and the calculated (T) and measured (T_m) period range for each measured SIW-train of a certain ebb slack

these waves cannot be generated by Maxworthy's mechanism (requiring $|u| < |c|$). So, are the SIWs generated by the Nash and Moum (2005) frontal generation mechanism? After all, the Texelstroom was inferred to be slightly stratified and may thus serve as a medium wherein frontally generated SIWs can propagate after fission from the Malzwin front once the SIW speed exceeds that of the decelerating front. But the resulting SIWs would then propagate in the direction of the gravity current (or front) (Nash and Moum 2005). Based on the measurements just before the wave appears, it is found that the front propagates nearly northward, along 5° T, which is roughly *opposite* to the wave. The frontal SIW generation mechanism is thus excluded too. Finally, the waves may also result purely from an instability of the negative shear flow. When the decreasing ebb current is near resonance, these waves might rapidly grow, to the extent of becoming nonlinear. This resonant generation mechanism may cause both up and downstream traveling SIWs. If we assume a linear, two-layer shear flow, we can show that circumstances are such that the SIWs might indeed be resonantly generated (Baines 1995). Using the linear long wave speed (da Silva and Helfrich 2008):

$$c_\pm = \frac{u_1 h_2 + u_2 h_1}{h_1 + h_2} \pm c_0 \left(1 - \frac{(u_2 - u_1)^2}{g'(h_1 + h_2)}\right)^{\frac{1}{2}}, \qquad (3)$$

with u_1 and u_2 velocities of the surface and bottom layer in along-wave direction, then the first and second term on the r.h.s. represent u and c, respectively, both corrected for vertical shear. Waves may be resonantly generated when the flow passes through the transcritical regime ($c_\pm \approx 0$) during the accelerating or decelerating phase of the tide. Though this is a linear model, it should be sufficiently detailed for us to judge if this mechanism is plausible.

In our case, we are in the decelerating tidal ebb phase, the signs of u and c are opposed, while $u > |c| > 0$. Thus, we deal with the case $c_+ > 0$, leading to *downstream* propagating SIWs, having longer wave periods than theoretically expected based on the KdV equation. Using the measurements to determine u_1 and u_2 and the layer depths and densities as before and defining a transcritical regime interval of Froude numbers $F = \left|\frac{u}{c}\right| \in [0.9\text{–}1.1]$, it is found that at the site of the deployment, the flow enters the transcritical regime about 17.5 min before the waves are measured. We therefore suggest that a while before the waves are measured, they have been resonantly generated further upstream and are subsequently advected downstream. Figure 2 seems to verify this idea showing wave bands upstream of the deployment location. Resonant generation and Doppler shifting, represented by the first term of the right-hand side of Eq. 3, can thus explain the observed wave period "inconsistency."

7 Discussion and conclusion

The ADCP measurements presented in this paper show intra-tidal processes that may influence tidally averaged circulation patterns. Using LSHA, a good approximation of tidally driven processes is found, which is well understood, especially for the along-stream direction. These coherent motions are subtracted from the measurements, leaving the incoherent current. The incoherent current is governed by many physical processes at different forcing frequencies. The combined processes lead to a complicated velocity structure in which individual effects are hard to separate (Scully and Friedrichs 2007; Souza and James 1996; Buijsman and Ridderinkhof 2008). Fortunately, temporary coherency is observed in the incoherent current, leading to three clearly defined, regularly occurring events, which are the transverse PLS, NLS, and SIWs.

The PLS and NLS appear almost instantly, mainly as changes in the vertical structure of the cross-stream velocity and ABI and seem to be associated with front passages. Because the Malzwin front will not be directed exactly in along-stream direction, the NLS will

have a component in the along-stream incoherent velocity. The combination of the measured changes in the ABI and cross-stream current suggest that cross-stream currents dominate the distribution of suspended matter in this phase of the tidal cycle in Marsdiep and will therefore influence sub-tidal distribution of sediments and nutrients.

The measured SIWs at site D, Fig. 2, propagate in southwesterly direction, out of Marsdiep. An inconsistency between theoretically calculated wave periods (using a KdV equation for two-layer stratification) and measured wave periods could only be resolved if waves propagate against the background current (u) but with a smaller speed ($c < u$), such that net wave motion and associated water transport are still in the same southwesterly direction of u. This was inconsistent with the Maxworthy (1979) topographic generation mechanism or with frontal generation from the Malzwin freshwater front (Nash and Moum 2005; Pan and Jay 2008; Marmorino and Smith 2007) but can be explained using resonant generation during the decelerating phase of the tidal cycle (da Silva and Helfrich 2008). This is not yet a commonly observed mechanism and thus provides an interesting case for further study.

There is multiple evidence for the appearance of SIWs in Marsdiep tidal channel. First, Fig. 1 shows pictures containing the surface expression of IWs on two different dates in region A of Fig. 2. Second, Fig. 2 shows the surface expression of IWs in regions A and B. Third, Fig. 4d shows measurements containing indications of IWs obtained from anchor station observations. Finally, SIWs were measured at location D of Fig. 2 with the deployment. The IWs in region B of Fig. 2 are spotted on a different date than the SIWs measured with the deployment. Nonetheless, we conclude both result from instability of the shear flow leading to resonant generation of infinitesimal waves at the interface between fresh Malzwin outflow surface layer and saline Wadden Sea water prompted by a change in depth or width of the tidal channel.

The surface expressions in region A of Fig. 2 and in the left picture of Fig. 1 are made on the same location during ebb slack, but on different days. While speculative, frequent observations from the ferry during ebb slack suggest that the IWs at this location propagate eastward into the Wadden Sea. This makes them into a second, separate group of IWs traveling *up-current*, thus oppositely directed to the measured SIWs at region B. The deep topographic feature "Helsdeur," Fig. 3b, in combination with the Maxworthy mechanism, might have given rise to this class of upstream traveling SIWs. Both groups of IWs at locations A and B in Fig. 2 thus depend on the same stratified Malzwin outflow during ebb currents but are generated at different locations and by different mechanisms.

Finally, additional data from 13 h ASs in Marsdiep throughout the past 6 years showed strong stratification either during ebb or flood slack. In particular, a few ASs also showed indications of mode one IWs during *flood* slacks (e.g., Fig. 4d). These can be identified as a third group of IWs (right panel of Fig. 1) propagating *out of* the Wadden Sea, which are likely related to the stratification caused by the intrusion of saline North Sea water into Marsdiep at flood, possibly again caused by Maxworthy's mechanism.

In summary, the combination of measurements, photographs, and visual observations described in the present paper makes the existence of (multiple sources of) SIWs in the Marsdiep channel undeniable. The occurrence of multiple sources of IWs in a relatively small area such as Marsdiep invites further study of (different) natural generation mechanisms. Also the observed SIWs lead to transport of water and thus of dissolved and floating material (as evidenced by variations in the ABI in Fig. 9 and by net transport in Fig. 10) and therefore act as a nutrient pump (Sandstrom and Elliott 1984). As a result, the SIWs may be important for the ecology of the Wadden Sea and are thus worth studying in more detail. In addition, the occurrence of SIWs in a highly energetic and dynamic estuary as the Marsdiep tidal channel indicates their inevitability in an area with stratification, strong but alternating tidal currents and uneven bottom topography. The intratidal motions (SIWs, PLS, and NLS), pronounced in the measurements, act on relatively short time scales compared to the semi-diurnal tidal period. Nonetheless, they are temporally dominant since fast transverse mixing processes, prompted by the presence of tidal channels adjacent to tidal flats, in combination with sheared longitudinal channel flow may lead to enhanced longitudinal spreading of watermasses, i.e., to shear dispersion (Zimmerman 1986). While typical Wadden Sea models are vertically integrated or, when 3D, mostly barotropic, to accurately reproduce all the intricate frontal dynamics unraveled by our observations, 3D baroclinic models are needed.

Acknowledgements The Ministry of Transport, Public Works and Water Management (Rijkswaterstaat) is thanked for the use of their bathymetry data. We thank Huib de Swart (IMAU, Utrecht University) for the helpful insights on estuarine circulation, José da Silva (University of Porto) for the helpful discussions on the resonant generation mechanism, the crew of RV Navicula for the help in deploying and gathering the deployment, and Frans Eijgenraam, Theo Hillebrand, Yvo Witte, and Jan Blom for their help designing and building the deployment. Finally, we thank Richard Koopman (TESO ferry) for providing observational information about Marsdiep.

References

Apel JR, Byrne HM, Proni JR, Charnell RL (1975) Observations of oceanic internal and surface-waves from earth resources technology satellite. J Geophys Res 80:865–881

Baines PG (1995) Topographic effects in stratified flows. Cambridge University Press, Cambridge, 482 pp

Bogucki D, Dickey T, Redekopp LG (1997) Sediment resuspension and mixing by resonantly-generated internal solitary waves. J Phys Oceanogr 27:1181–1196

Bowden KF, Gilligan RM (1971) Characteristic features of estuarine circulation as represented in the Mersey estuary. Limnol Oceanogr 16:490–502

Buijsman MC, Ridderinkhof H (2007a) Long-term ferry-ADCP observations of tidal currents in the Marsdiep inlet. J Sea Res 57:237–256

Buijsman MC, Ridderinkhof H (2007b) Water transport at subtidal frequencies in the Marsdiep inlet. J Sea Res 58:255–268

Buijsman MC, Ridderinkhof H (2008) Variability of secondary currents in a weakly stratified tidal inlet with low curvature. Cont Shelf Res 28:1711–1723

Burchard H, Baumert H (1998) The formation of estuarine turbidity maxima due to density effects in the salt wedge. A hydrodynamic process study. J Phys Oceanogr 28:309–321

Burchard H, Hetland RD, Fischer E, Schuttelaars HM (2011) Drivers of residual circulation in tidally energetic estuaries: straight and irrotational estuaries with parabolic cross-section. J Phys Oceanogr 41:548–570

Chant RJ (2002) Secondary circulation in a region of flow curvature: relationship with tidal forcing and river discharge. J Geophys Res 107:3131

Cresswell G, Zhou C, Tildesley PC, Nilsson CS (1996) SAR observations of internal wave wakes from sea mounts. Mar Freshw Res 47:489–495

da Silva JCB, Helfrich KR (2008) Synthetic aperture radar observations of resonantly generated internal solitary waves at race point channel (cape cod). J Geophys Res 113:252–262

De Boer GJ, Pietrzak JD, Winterwerp JC (2006) On the vertical structure of the Rhine region of freshwater influence. Ocean Dyn 56:198–216

Defant A (1961) Physical oceanography, vol 2. Pergamon, New York, p viii + 598 pp

Deines KL (1999) Backscatter estimation using broadband acoustic Doppler current profilers. In: Anderson S, Terray E, White J, Williams A (eds) Proceedings of the IEEE sixth working conference on current measurement, San Diego, pp 249–253

Dyer KR (1973) Estuaries: a physical introduction. Wiley, Aberdeen, 140 pp

Dyer KR (1982) Mixing caused by lateral internal seiching within a partially mixed estuary. Estuar Coast Shelf Sci 15:443–452

Emery WJ, Thomson RE (2001) Data analysis methods in physical oceanography. Elsevier, Amsterdam, 654 pp

Farmer DM, Armi L (1999) The generation and trapping of solitary waves over topography. Science 283:188–190

Farmer DM, Smith JD (1980) Tidal interaction of stratified flow with a sill in knight inlet. Deep-Sea Res A Oceanogr Res Pap 27:239–246

Fu LL, Holt B (1984) Internal waves in the Gulf of California: observations from a spaceborne radar. J Geophys Res 89:2053–2060

Gerkema T, Zimmerman JTF (2008) An introduction to internal waves. Lecture Notes, Royal NIOZ, Texel, 207 pp

Geyer WR, Smith JD (1987) Shear instability in a highly stratified estuary. J Phys Oceanogr 17:1668–1679

Geyer WR, Trowbridge JH, Bowen MM (2000) The dynamics of a partially mixed estuary. J Phys Oceanogr 30:2035–2048

Hansen DV, Rattray M (1966) New dimensions in estuary classification. Limnol Oceanogr 11:319–326

Hughes BA, Grant HL (1978) The effect of internal waves on surface wind waves 1. Experimental measurements. J Geophys Res 83:443–454

Huijts KMH, Schuttelaars HM, de Swart HE, Friedrichs CT (2009) Analytical study of the transverse distribution of along-channel and transverse residual flows in tidal estuaries. Cont Shelf Res 29:89–100

Kalkwijk JPT, Booij R (1986) Adaption of secondary flow in nearly-horizontal flow. J Hydraul Res 24:19–37

LeBlond PH, Mysak LA (1978) Waves in the ocean. Elsevier, Amsterdam, 602 pp

Lerczak JA, Geyer WR (2004) Modeling the lateral circulation in straight, stratified estuaries. J Phys Oceanogr 34:1410–1428

Maas LRM, Van Haren JJM (1987) Observations on the vertical structure of tidal and inertial currents in the central North Sea. J Mar Res 45:293–318

MacCready P (2004) Toward a unified theory of tidally-averaged estuarine salinity structure. Estuaries 27:561–570

MacCready P, Geyer WR (2010) Advances in estuarine physics. Ann Rev Mar Sci 2:35–58

Marmorino G, Smith G (2007) Infrared imagery of a turbulent intrusion in a stratified environment. Estuar Coast 30:671–678

Maxworthy T (1979) Note on the internal solitary waves produced by tidal flow over a three-dimensional ridge. J Geophys Res 84:338–346

Nash JD, Moum JN (2005) River plumes as a source of large-amplitude internal waves in the coastal ocean. Nature 437:400–403

Neilson BJ, Kuo A, Brubaker J (eds) (1989) Estuarine circulation. Humana, Clifton, 377 pp

Neumann G, Pierson W Jr (1966) Principles of physical oceanography. Prentice Hall, Englewood Cliffs, 545 pp

New AL, Dyer KR, Lewis RE (1987) Internal waves and intense mixing periods in a partially stratified estuary. Estuar Coast Shelf Sci 24:15–33

Osborne AR, Burch TL (1980) Internal solitons in the Andaman Sea. Science 208:451–460

Ostrovsky LA, Stepanyants YA (1989) Do internal solutions exist in the ocean? Rev Geophys 27:293–310

Pan J, Jay DA (2008) Dynamic characteristics and horizontal transports of internal solitons generated at the Columbia River plume front. Cont Shelf Res 29:252–262

Postma H (1954) Hydrography of the Dutch Wadden Sea. Arch Neerl Zool 10:405–511

Prandle D (1982) The vertical structure of tidal currents and other oscillatory flows. Cont Shelf Res 1:191–207

Pritchard DW (1952) Salinity distribution and circulation in the Chesapeake Bay estuaries system. J Mar Res 11:106–123

Pritchard DW (1954) A study of the salt balance in a coastal plain estuary. J Mar Res 13:133–144

Pritchard DW (1956) The dynamic structure of a coastal plain estuary. J Mar Res 15:33–42

Pritchard DW (1989) Estuarine classification—a help or a hindrance? In: Neilson B, Kuo A, Brubaker J (eds) Estuarine circulation. Humana, Clifton, pp 1–38

Ridderinkhof H (1988a) Tidal and residual flows in the Western Dutch Wadden Sea I: numerical model results. Neth J Sea Res 22:1–21

Ridderinkhof H (1988b) Tidal and residual flows in the Western Dutch Wadden Sea II: an analytical model to study the

constant flow between connected tidal basins. Neth J Sea Res 22:185–198
Roberts J (1975) Internal gravity waves in the ocean. Marcel Dekker, New York, 274 pp
Sandstrom H, Elliott JA (1984) Internal tide and solitons on the Scotian Shelf: a nutrient pump at work. J Geophys Res 89:6415–6426
Scully ME, Friedrichs CT (2007) The importance of tidal and lateral asymmetries in stratification to residual circulation in partially mixed estuaries. J Phys Oceanogr 37:1496–1511
Scully ME, Geyer WR, Lerczak JA (2009) The influence of lateral advection on the residual estuarine circulation: a numerical modeling study of the Hudson River Estuary. J Phys Oceanogr 39:107–124
Simpson JH, Brown J, Matthews J, Allen G (1990) Tidal straining, density currents, and stirring in the control of estuarine stratification. Estuar Coast 13:125–132
Souza AJ, James ID (1996) A two-dimensional (x-z) model of tidal straining in the Rhine ROFI. Cont Shelf Res 16:949–966
Stacey MT, Burau JR, Monismith SG (2001) Creation of residual flows in a partially stratified estuary. J Geophys Res 106: 13–37
Walters RA (1989) A tale of two estuaries: Columbia Bay, Alaska, and San Francisco Bay, California. In: Neilson B, Kuo A, Brubaker J (eds) Estuarine circulation. Humana, Clifton, pp 183–200
Wang D (2006) Tidally generated internal waves in partially mixed estuaries. Cont Shelf Res 26:1469–1480
Winant CD (2007) Three-dimensional tidal flow in an elongated, rotating basin. J Phys Oceanogr 37:2345–2362
Wright L, Yang Z, Bornhold B, Keller G, Prior D, Wiseman W, Fan Y, Su Z (1986) Short period internal waves over the Huanghe (Yellow River) delta front. Geo Mar Lett 6:115–120
Zimmerman JTF (1976a) Mixing and flushing of tidal embayments in the Western Dutch Wadden Sea, part I: description of salinity distribution and calculation of mixing time scales. Neth J Sea Res 10:149–191
Zimmerman JTF (1976b) Mixing and flushing of tidal embayments in the Western Dutch Wadden Sea, part II: analysis of mixing processes. Neth J Sea Res 10:397–439
Zimmerman JTF (1986) The tidal whirlpool: a review of horizontal dispersion by tidal and residual currents. Neth J Sea Res 20:133–154